AIMS Mathematics

http://www.aimspress.com/journal/Math

AIMS Mathematics, 5(1): 216–225.
DOI:10.3934/math.2020013
Received: 28 October 2019
Accepted: 01 November 2019
Published: 04 November 2019

Research article

Mathematical modeling of brain metabolites variations in the circadian rhythm

Laura Hatchondo[1], Carole Guillevin[2,3], Mathieu Naudin[2,3], Laurence Cherfils[4], Alain Miranville[2,*] and Rémy Guillevin[2,3]

[1] Université de Poitiers, Laboratoire de Mathématiques et Applications, Equipe DACTIM-MIS, UMR CNRS 7348, 11 Boulevard Marie et Pierre Curie, Site du Futuroscope, Téléport 2, Bâtiment H3 - TSA 61125, F-86073 Poitiers Cedex 9, France

[2] Université de Poitiers, Laboratoire I3M et Laboratoire de Mathématiques et Applications, Equipe DACTIM-MIS, UMR CNRS 7348, 11 Boulevard Marie et Pierre Curie, Site du Futuroscope, Téléport 2, Bâtiment H3 - TSA 61125, F-86073 Poitiers Cedex 9, France

[3] CHU de Poitiers, 2 Rue de la Milétrie, F-86021 Poitiers, France

[4] Université de La Rochelle, Laboratoire des Sciences de l'Ingénieur pour l'Environnement, UMR CNRS 7356, Avenue Michel Crépeau, F-17042 La Rochelle Cedex, France

* **Correspondence:** Email: Alain.Miranville@math.univ-poitiers.fr; Tel: +33549496891; Fax: +33549496901.

Abstract: Our aim in this paper is to study ODEs models in view of applications to brain metabolites variations in the circadian rhythm. We address the well-posedness of the models, as well as the nonnegativity of the solutions. We then give numerical simulations which we compare with real medical data.

Keywords: circadian rhythm; brain metabolites variations; mathematical modeling; nonnegativity; simulations
Mathematics Subject Classification: 34A12, 92C50

1. Introduction

Magnetic resonance human imaging has emerged 30 years ago and progressively imposed itself as the reference for in vivo noninvasive multiorgans investigation. Recent and huge developments of technical aspects and sequences have lead MRI to switch from "anatomic" to multiparametric powerful investigation system. Namely, multinuclear spectroscopy/imaging and perfusion sequences

today provide numerous so called "metabolic" information which match with tremendous increase of human metabolism knowledge (see [2, 5]).

Then, significant metabolic modifications have been demonstrated in pathologies usually presenting a normal "anatomic" appearance, such as psychiatric diseases (see [1, 3]). The correlative (and underlying) question concerned the measurements' reliability. Yet circadian variations of metabolite concentrations, as they can be calculated from spectroscopic acquisitions, appeared to be of importance in this context.

We performed three successive acquisitions at "key" moments referring to the circadian rhythm, 7.30 am, 1.30 pm and 5.30 pm, on 30 healthy volunteers and on 12 different areas in the brain. Several fluctuations were found within acquisition time and location, thus suggesting modeling usefulness.

We propose hereafter to develop a mathematical analysis and modeling for describing and integrating these fluctuations. More precisely, we consider models of the form

$$y' + \frac{ky}{k' + y} = a \sin(bt + c),\ a,\ b,\ k,\ k' > 0,$$

$$y' + \frac{ky}{k' + y} = a \sin^2(bt + c),\ a,\ b,\ k,\ k' > 0,$$

with a symport nonlinear term (see [4]). Here, u is a metabolite's concentration, e.g., lactate. We give a mathematical analysis of these models; the main difficulty is the (expected) nonnegativity of the concentration. We then present numerical simulations which we compare with the medical data mentioned above.

2. Mathematical analysis

We consider the initial value problem

$$y' + \frac{ky}{k' + y} = a \sin(bt + c),\ a,\ b,\ k,\ k' > 0, \tag{2.1}$$

$$y(0) = y_0 \geq 0. \tag{2.2}$$

Noting that the function

$$f : (t, x) \mapsto a \sin(bt + c) - \frac{kx}{k' + x}$$

is C^1 on $\mathbb{R} \times (-k', +\infty)$, it follows from the Cauchy–Lipschitz theorem that (2.1)-(2.2) possesses the maximal solution

$$y : [0, T_\star) \to (-k', +\infty).$$

We have the

Theorem 2.1. *The maximal solution y is defined on $\mathbb{R}^+$ (i.e., $T_\star = +\infty$).*

Proof. Let y_+ be the maximal solution to the initial value problem

$$y'_+ + \frac{ky_+}{k' + |y_+|} = a, \tag{2.3}$$

$$y_+(0) = y_0. \tag{2.4}$$

Noting that the function

$$g : x \mapsto \frac{kx}{k' + |x|}$$

is of class C^1 and globally Lipschitz continuous on $\mathbb{R}$, it follows that y_+ is uniquely defined on $\mathbb{R}^+$. Multiplying (2.3) by $-y_+^-$, where $y_+ = y_+^+ - y_+^-$, $y_+^+ = \max(y_+, 0)$, $y_+^- = \max(-y_+, 0)$, we obtain

$$\frac{1}{2}\frac{d}{dt}|y_+^-|^2 + \frac{k|y_+^-|^2}{k' + |y_+|} = -ay_+^- \leq 0,$$

so that

$$\frac{d}{dt}|y_+^-|^2 \leq 0.$$

Therefore

$$|y_+^-| = 0$$

and

$$y_+ \geq 0. \tag{2.5}$$

This yields that y_+ is the unique solution to

$$y'_+ + \frac{ky_+}{k' + y_+} = a, \tag{2.6}$$

$$y_+(0) = y_0, \tag{2.7}$$

defined on $\mathbb{R}^+$.

Let then y_- be the maximal solution to

$$y'_- + \frac{ky_-}{k' + y_-} = -a, \tag{2.8}$$

$$y_-(0) = y_0, \tag{2.9}$$

defined on $[0, T_\star^-)$ (the existence and uniqueness of y_- follows from the Cauchy–Lipschitz theorem). We can note that (2.8) possesses a unique equilibrium defined by

$$\frac{ky_-^e}{k' + y_-^e} = -a,$$

i.e.,

$$y_-^e = -\frac{ak'}{a+k} \in (-k', 0).$$

Setting $z = y_- - y_-^e$, we have

$$z' + \varphi_-(t)z = 0,$$

where

$$\varphi_-(t) = \int_0^1 h'(sy_- + (1-s)y_-^e)\, ds \geq 0,$$

with $h(x) = \frac{kx}{k'+x}$. Therefore,

$$z(t) = z(0)e^{-\int_0^t \varphi_-(\xi)\, d\xi}$$

and

$$y_-(t) = y_-^e + (y_0 - y_-^e)e^{-\int_0^t \varphi_-(\xi)\, d\xi},\ t \geq 0. \tag{2.10}$$

This yields that y_- is bounded, so that $T_\star^- = +\infty$ and

$$y_-(t) > -k',\ t \geq 0. \tag{2.11}$$

Now, it follows from the comparison principle that, $\forall t \in [0, T_\star)$,

$$y_-(t) \leq y(t) \leq y_+(t). \tag{2.12}$$

In particular, if $T_\star < +\infty$, then y remains bounded as $t \to T_\star$, which yields a contradiction. Thus, $T_\star = +\infty$, which finishes the proof.

□

Remark 2.2. We can actually prove, proceeding as above, that $y(t) \geq y_-^e$, $t \geq 0$. Indeed, we have, setting $z = y - y_-^e$,

$$z' + g(y) - g(y_-^e) = a + a\sin(bt + c) \geq 0.$$

Multiplying the above equality by $-z^-$, we obtain

$$\frac{1}{2}\frac{d}{dt}|z^-|^2 - (g(y) - g(y_-^e))z^- \leq 0,$$

which yields, noting that $g' \geq 0$ and $-zz^- = |z^-|^2$,

$$\frac{d}{dt}|z^-|^2 \leq 0$$

and the result follows. Note however that (2.10) gives a better lower bound on y, in the sense that it yields that y is nonnegative at least for some time. Note indeed that y corresponds to a concentration and is expected to be nonnegative (see below).

We then have the

Theorem 2.3. *We assume that $k > a$. Then the solution y to* (2.1)-(2.2) *(defined on $\mathbb{R}^+$) is bounded.*

Proof. We again consider the solution y_+ to (2.6)-(2.7), defined on $\mathbb{R}^+$. Note that, when $k > a$, (2.6) possesses a unique equilibrium y_+^e defined by

$$\frac{ky_+^e}{k' + y_+^e} = a,$$

i.e.,

$$y_+^e = \frac{ak'}{k-a} > 0.$$

Proceeding as in the proof of Theorem 2.1, we find

$$y_+(t) = y_+^e + (y_0 - y_+^e)e^{-\int_0^t \varphi_+(\xi)\,d\xi},\ t \geq 0, \tag{2.13}$$

where

$$\varphi_+(t) = \int_0^1 g'(sy_+ + (1-s)y_+^e)\,ds \geq 0. \tag{2.14}$$

Therefore, y_+ is bounded and, recalling (2.12), it follows that y is bounded, which finishes the proof of the theorem.

□

Actually, assuming that y_0 is large enough, we can also prove that y is bounded on $\mathbb{R}^+$. More precisely, we have the

Theorem 2.4. *We assume that*

$$y_0 \geq 2\frac{a}{b}. \tag{2.15}$$

Then, the solution y to (2.1)-(2.2) *is bounded.*

Proof. Let now y_+ be the solution (defined on $\mathbb{R}^+$) to

$$y_+' = a\sin(bt + c), \tag{2.16}$$

$$y_+(0) = y_0. \tag{2.17}$$

Clearly,

$$y_+(t) = y_0 + \frac{a}{b}(\cos c - \cos(bt + c)), \tag{2.18}$$

so that

$$y_+(t) \geq 0,\ t \geq 0. \tag{2.19}$$

Next, we set $z = y - y_+$ and have

$$z' + \frac{ky}{k' + y} = 0,\ z(0) = 0,$$

which we can rewrite as

$$z' + \frac{kz}{k' + y} = -\frac{ky_+}{k' + y}. \tag{2.20}$$

Multiplying (2.20) by z^+, we obtain

$$\frac{1}{2}\frac{d}{dt}|z^+|^2 + \frac{k|z^+|^2}{k' + y} = -\frac{ky_+z^+}{k' + y},$$

which yields, noting/recalling that $k' + y > 0$ and $y_+ \geq 0$,

$$\frac{d}{dt}|z^+|^2 \leq 0,$$

so that

$$y(t) \leq y_+(t),\ t \geq 0.$$

Employing once more the comparison principle, we deduce that

$$y_-(t) \leq y(t) \leq y_+(t),\ t \geq 0, \tag{2.21}$$

where y_- is as defined in the proof of Theorem 2.1. The proof follows from (2.21).

□

Remark 2.5. One crucial question is whether the solution y to (2.1)-(2.2) remains nonnegative, assuming that $y_0 > 0$ (note indeed that, if, for some $t \geq 0$, $y(t) = 0$, then

$$y'(t) = a\sin(bt + c)$$

and can be negative; in particular, if $y_0 = 0$ and $\sin c < 0$, then $y'(0) < 0$); as already mentioned, y corresponds to a concentration and is thus expected to be nonnegative. We thus see that y can be negative when $y_0 = 0$ (and even when $y_0 > 0$ is small). We believe however that, when $y_0 > 0$ is large enough, then y remains positive; this is confirmed by the numerical simulations below. Unfortunately, we have not been able to prove this. One difficulty is to find a nonnegative subsolution.

Remark 2.6. A model, ensuring nonnegativity, reads

$$y' + \frac{ky}{k' + y} = a\sin^2(bt + c),\ a,\ b,\ k,\ k' > 0, \tag{2.22}$$

$$y(0) = y_0 \geq 0. \tag{2.23}$$

As above, we have the existence and uniqueness of the solution, defined on $\mathbb{R}^+$, such that $y(t) > -k'$, $t \geq 0$. Then, multiplying (2.22) by $-y^-$, we obtain

$$\frac{1}{2}\frac{d}{dt}|y^-|^2 + \frac{k|y^-|^2}{k' + y} = -a\sin^2(bt + c)y^- \leq 0,$$

so that

$$\frac{d}{dt}|y^-|^2 \leq 0$$

and

$$y(t) \geq 0,\ t \geq 0.$$

The numerical simulations below show that this model gives satisfactory results for the lactate concentrations (the solution to the first model becomes indeed negative in that case). We can also note that, as far as the other metabolites concentrations are concerned, the first model matches better the experimental data. However, it is less precise for predicting the longtime behavior of the concentrations.

3. Numerical simulations

3.1. Using model (2.1)

We test model (2.1) with medical data, supplied from MRI scans by the Poitiers University Hospital (see the introduction). These data consist, for several patients, in the concentrations of brain metabolites (e.g., lactate, choline) at different brain areas and at different times of the day: 7.30 am, 1.30 pm and 5.30 pm. Basically, these data can be divided into four classes: the hat shape (the second dosage is maximal), the reverse hat shape (the second dosage is minimal), the increasing shape (the three dosages increase with respect to time) and the decreasing shape.

In Figure 1, we present, for each class of data, a comparison between the medical data and the simulations, during the ten hours (left) and during the three days (right) next to the first MRI scan. In the right columns of Figure 1, the blue circles correspond to actual measured data, and the red crosses correspond to predicted values, taking into account the circadian rhythm. The first row of the figure corresponds to a choline dosage, for a patient of the hat shape class. The corresponding model is $y'(t) = -\frac{0.007y}{10.5+y} + 0.5\sin(0.265t + 1.4)$. The second row corresponds to a choline dosage, for a patient of the reverse hat shape class, with the model $y'(t) = -\frac{0.01y}{5+y} + 0.5\sin(0.265t - 0.85)$. The third row corresponds to a choline dosage, for a patient of the increasing shape class, with the model $y'(t) = -\frac{0.004y}{0.8+y} + 0.29\sin(0.265t + 1)$. Finally, the fourth row corresponds to a Cr dosage for a patient of the decreasing shape class, and the model is $y'(t) = -\frac{0.004y}{7+y} + 0.3\sin(0.265t + 2.8)$. Figure 1 shows that the model matches well the medical data.

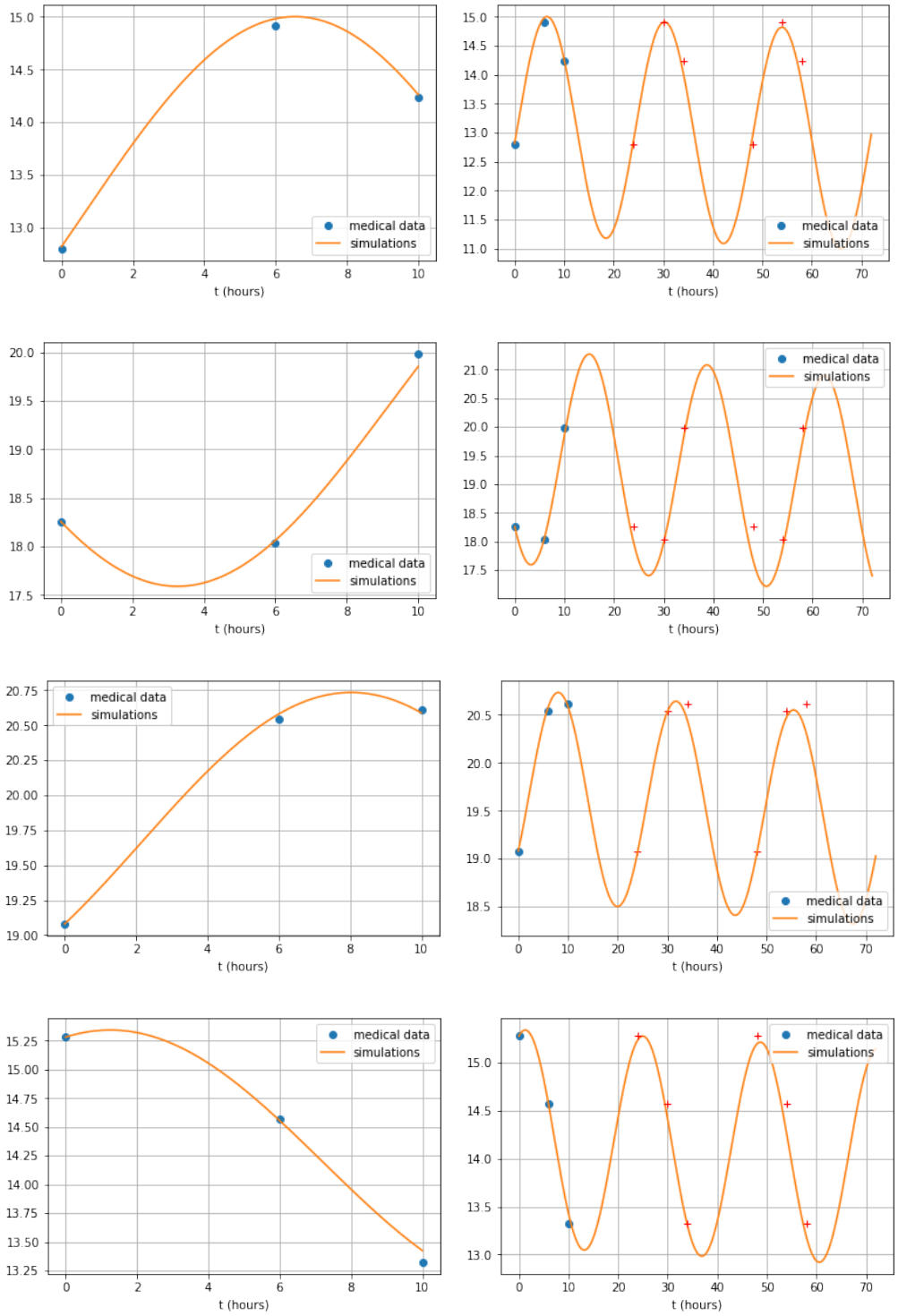

Figure 1. Comparisons between the medical data and the simulations, during the first 10 hours (left column) and during the three days (right column) next to the first MRI scan. First row: choline dosage for a patient of the hat shape class; second row: choline dosage for a patient of the reverse hat shape class; third row: choline dosage for a patient of the increasing shape class; and fourth row: choline dosage for a patient of the decreasing shape class.

3.2. *Using model* (2.22)

Although model (2.1) seems convenient in many cases, it is not suitable for modeling the variations of lactate. Indeed, the concentrations being small for this metabolite, the simulations may become negative during the simulations. In Figure 2, we compare, in the case of a lactate concentration, two solutions given by the models (2.1) ($y'(t) = -\frac{0.11y}{8+y} + 0.5\sin(0.265t + 1.9)$) and (2.22) ($y'(t) = -\frac{2y}{5.5+y} + 0.9\sin^2(0.265t + 0.9)$). With the first model, the solutions become negative after ten hours, while, with the second one, the solutions remain positive (see Remark (2.6)).

In Figure 3, we compare, for a choline concentration, two solutions : one given by model (2.1) ($y'(t) = -\frac{0.007y}{10.5+y} + 0.5\sin(0.265t + 1.4)$) and the second one given by model (2.22) ($y'(t) = -\frac{0.7y}{10.7+y} + 0.8\sin^2(0.1325t+1.4)$). As far as the first ten hours are concerned, the solutions are very similar (Figure 2, left). Furthermore, although both solutions match well the medical data, they are very different after the three days period (right). In particular, the range of variations of the solution of model (2.1) is significantly larger than the one for model (2.22) and may be less medically relevant.

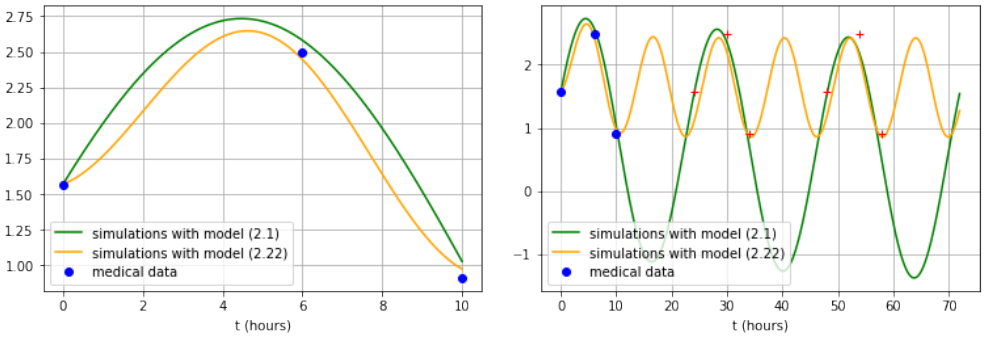

Figure 2. Comparison of the simulations obtained with model (2.1) and (2.22) for a lactate concentration.

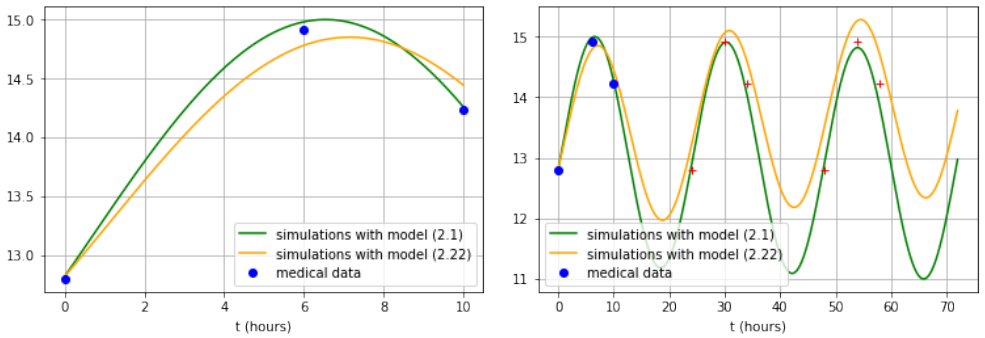

Figure 3. Comparison of the simulations obtained with model (2.1) and (2.22) for a choline concentration.

Conflict of interest

The authors declare no conflicts of interest in this paper.

References

1. B. P. Brennan, S. L. Rauch, J. E. Jensen, et al. *A critical review of magnetic resonance spectroscopy studies of obsessive-compulsive disorder*, Biol. Psychiat., **73** (2013), 24–31.
2. R. Guillevin, C. Menuel, J.-N. Vallée, et al. *Mathematical modeling of energy metabolism and hemodynamics of WHO grade II gliomas using in vivo MR data*, CR Biol., **334** (2011), 31–38.
3. L. Hatchondo, N. Jaafari, N. Langbour, et al. ^{1}*H magnetic resonance spectroscopy suggests neural membrane alteration in specific regions involved in obsessive-compulsive disorder*, Psychiatry Res. Neuroimaging, **269** (2017), 48–53.
4. J. Keener and J. Sneyd, *Mathematical physiology*, Second edition, Interdisciplinary Applied Mathematics, Springer-Verlag, New York, 2009.
5. M. Law, S. Yang, H. Wang, et al. *Glioma grading: sensitivity, specificity, and predictive values of perfusion MR imaging and proton MR spectroscopic imaging compared with conventional MR imaging*, Am. J. Neuroradiol., **24** (2003), 1989–1998.

AIMS Press